

# Simulated microgravity using the Random Positioning Machine inhibits differentiation and alters gene expression profiles of 2T3 preosteoblasts

Steven J. Pardo,<sup>1\*</sup> Mamta J. Patel,<sup>1\*</sup> Michelle C. Sykes,<sup>1</sup> Manu O. Platt,<sup>1</sup> Nolan L. Boyd,<sup>1</sup> George P. Sorescu,<sup>1</sup> Min Xu,<sup>3</sup> Jack J. W. A. van Loon,<sup>4</sup> May D. Wang,<sup>1</sup> and Hanjoong Jo<sup>1,2</sup>

<sup>1</sup>Wallace H. Coulter Department of Biomedical Engineering, Georgia Institute of Technology and Emory University, Atlanta; <sup>2</sup>Division of Cardiology, Department of Medicine, Emory University School of Medicine, Atlanta, Georgia; <sup>3</sup>Amersham Biosciences, Piscataway, New Jersey; and <sup>4</sup>Dutch Experiment Support Center, Department of Oral Biology, Academic Center for Dentistry Amsterdam, Free University, Amsterdam, The Netherlands

Submitted 5 May 2004; accepted in final form 29 January 2005

**Pardo, Steven J., Mamta J. Patel, Michelle C. Sykes, Manu O. Platt, Nolan L. Boyd, George P. Sorescu, Min Xu, Jack J. W. A. van Loon, May D. Wang, and Hanjoong Jo.** Simulated microgravity using the Random Positioning Machine inhibits differentiation and alters gene expression profiles of 2T3 preosteoblasts. *Am J Physiol Cell Physiol* 288: C1211–C1221, 2005. First published February 2, 2005; doi:10.1152/ajpcell.00222.2004.—Exposure to microgravity causes bone loss in humans, and the underlying mechanism is thought to be at least partially due to a decrease in bone formation by osteoblasts. In the present study, we examined the hypothesis that microgravity changes osteoblast gene expression profiles, resulting in bone loss. For this study, we developed an in vitro system that simulates microgravity using the Random Positioning Machine (RPM) to study the effects of microgravity on 2T3 preosteoblast cells grown in gas-permeable culture disks. Exposure of 2T3 cells to simulated microgravity using the RPM for up to 9 days significantly inhibited alkaline phosphatase activity, recapitulating a bone loss response that occurs in real microgravity conditions without altering cell proliferation and shape. Next, we performed DNA microarray analysis to determine the gene expression profile of 2T3 cells exposed to 3 days of simulated microgravity. Among 10,000 genes examined using the microarray, 88 were downregulated and 52 were upregulated significantly more than twofold using simulated microgravity compared with the static 1-g condition. We then verified the microarray data for some of the genes relevant in bone biology using real-time PCR assays and immunoblotting. We confirmed that microgravity downregulated levels of alkaline phosphatase, runt-related transcription factor 2, osteomodulin, and parathyroid hormone receptor 1 mRNA; upregulated cathepsin K mRNA; and did not significantly affect bone morphogenic protein 4 and cystatin C protein levels. The identification of gravisensitive genes provides useful insight that may lead to further hypotheses regarding their roles in not only microgravity-induced bone loss but also the general patient population with similar pathological conditions, such as osteoporosis.

microarray; bone loss; alkaline phosphatase; *runx2*; osteomodulin

THERE IS INCREASING INTEREST in human space exploration, including extensive trips to deep-space planets such as Mars. However, the harsh outer space environment, consisting of microgravity and radiation, poses significant health risks for astronauts. For example, microgravity conditions in space have been shown to cause decreased bone mass (5, 6, 9, 14), bone demineralization (7, 33, 36), skeletal muscle atrophy (23),

cardiovascular deconditioning (2, 38), and immune dysfunction (30). Many of these pathophysiological changes cannot yet be counteracted adequately by physical exercise (18) or nutritional supplementation alone (6, 12, 34). Therefore, it is imperative to understand the mechanisms of microgravity-induced pathophysiology so that human space exploration can continue with minimal negative effects on astronauts. Furthermore, our knowledge of the mechanisms of inducing spaceflight-dependent health problems may also provide insights into the understanding of pathophysiology occurring in the general population, including osteoporosis, muscle atrophy, and cardiovascular deconditioning.

Unfortunately, it has been difficult and impractical to conduct well-controlled in vitro studies in sufficient numbers in real microgravity conditions because of the limited and expensive nature of spaceflight missions. Thus, to investigate pathophysiology during spaceflight, several ground-based systems, including the two-dimensional (2-D) and three-dimensional (3-D) clinostats and the rotating wall vessel, have been developed to simulate microgravity using cultured cells and tissues (1, 19, 24, 29). Simulated microgravity is based on the hypothesis that sensing no weight would have effects similar to those of weightlessness (13). The 3-D clinostat simulates microgravity by continuously moving the gravity vector in three dimensions before the cell has enough time to sense it, which is a method called gravity-vector averaging.

Previous studies have indicated that spaceflight-induced bone loss may be due in part to decreased osteoblastic function with or without enhancing osteoclastic bone resorption (8). Using 2-D clinostats and rotating wall vessels, simulated microgravity has been shown to inhibit markers of bone mass formation such as alkaline phosphatase (*alp*) activity and runt-related transcription factor 2 (*runx2*) activity (24, 42). While these studies examined only a few candidate genes that are likely to be involved in bone mass regulation, systematic and unbiased characterization of gene expression profiles scanning the majority of genes has not been performed. In the present study, we hypothesized that bone loss due to simulated microgravity is regulated by preosteoblastic gene expression, which inhibits differentiation of the preosteoblasts into mature osteoblasts.

To test this hypothesis, we 1) developed and characterized an in vitro cell culture system using preosteoblast cells (2T3)

\* S. J. Pardo and M. J. Patel contributed equally to this work.

Address for reprint requests and other correspondence: H. Jo, Wallace H. Coulter Dept. of Biomedical Engineering, Georgia Institute of Technology and Emory Univ., 308D WMB, Atlanta, GA 30322 (E-mail: hanjoong.jo@bme.gatech.edu).

The costs of publication of this article were defrayed in part by the payment of page charges. The article must therefore be hereby marked "advertisement" in accordance with 18 U.S.C. Section 1734 solely to indicate this fact.

exposed to simulated microgravity conditions produced by a 3-D clinostat called the Random Positioning Machine (RPM), 2) examined the cell proliferation and the alkaline phosphatase activities of 2T3 cells, 3) performed DNA microarray studies, and 4) validated the microarray data using quantitative real-time PCR and immunoblotting.

## METHODS

**Cell culture.** 2T3 murine osteoblast precursor cells were kindly provided by Dr. Xu Cao of the University of Alabama at Birmingham (40). The cells were cultured in a growth medium [ $\alpha$ -minimal essential medium containing 10% fetal bovine serum (Atlanta Biologicals) with 100 U/ml penicillin and 100  $\mu$ g/ml streptomycin] in a standard humidified incubator (37°C, 5% CO<sub>2</sub>).

**Cell seeding into OptiCells and simulated microgravity studies.** Confluent 2T3 cells grown in T-75 flasks were trypsinized using 0.05% trypsin-EDTA (Sigma), and 2 million cells were seeded into a gas-permeable cell culture disk (OptiCell) according to the manufacturer's instructions. As shown in Fig. 1A, an OptiCell disk is a sealed cell culture disk encapsulated by two optically clear, gas-permeable polystyrene membranes containing two ports that allow access to the contents of the OptiCell. The internal disk dimensions are 74.8  $\times$  65  $\times$  2.06 mm, and they can be filled with 10–14 ml of medium. To seed cells on both membranes on each side of the OptiCell, the disks were turned over every 5 min for 1 h. Cells were then grown for 3 days to confluence in 14 ml of growth medium before exposure to the stimulus. The day on which the OptiCells were mounted on the RPM was referred to as *day 0*. On *day 0*, the medium was replaced with 14 ml of fresh growth medium, and all of the air bubbles were removed. We found removing the air bubbles to be a critical step in preventing potentially uncharacterized mechanical perturbation during RPM exposure.

**Random Positioning Machine.** A desktop RPM described by Huijser (15) and manufactured by Fokker Space was used to simulate microgravity. As shown in Fig. 1B, the dimensions of the RPM are 30  $\times$  30  $\times$  30 cm with inner and outer frames that are independently controlled by two different motors. The OptiCell disks were mounted on the center of the platform located on the inner frame, and a maximum of eight disks were used in each microgravity experiment. The RPM was operated in random modes of speed and direction (0.1–2 rad/s) via a computer user interface with dedicated control software inside a humidified incubator (5% CO<sub>2</sub> at 37°C). Under this

experimental condition, the cells were exposed to simulated microgravity conditions ranging from 0 to 0.01 g (15). For static 1-g controls, OptiCell disks seeded at the same time as the microgravity disks were placed into the same incubator as the RPM. Samples were harvested at *days 0, 1, 3, 5, 7, and 9*. For a 3-day experiment, the OptiCells were exposed to the simulated microgravity condition without interruption because no medium change was necessary during this period. For experiments taking >3 days, however, the medium was changed every 3 days (*days 3 and 6*) by stopping the RPM for ~20 min before restarting it.

**Cell proliferation assay.** To determine cell proliferation, attached cells were collected by trypsinization after experimental treatments, and cell numbers were determined using an aliquot of cell suspension and counted with a Coulter counter.

**Alkaline phosphatase assay.** After collecting culture medium following exposure to the simulated gravity, cells were scraped in 500  $\mu$ l of lysis buffer containing 0.2% Nonidet P-40 in 1 mM MgCl<sub>2</sub> and stored at –80°C until needed. Alkaline phosphatase (ALP) activity was determined using a Diagnostics ALP assay kit (Sigma) according to the manufacturer's instructions (26). Aliquots of lysate (20  $\mu$ l) and *p*-nitrophenol standard (Sigma) were used for the assay.

**RNA isolation, reverse transcription, and quantitative real-time PCR.** Total RNA was prepared by using the RNeasy Mini kit (Qiagen) and reverse transcribed by using random primers and a SuperScript II kit (Life Technologies) (31). The synthesized and purified cDNA was amplified using a LightCycler (Roche Applied Science), and the size of each PCR product was verified by performing agarose gel electrophoresis as we described previously (31). The mRNA copy numbers were determined on the basis of standard curves generated with the genes of interest and 18S templates. The 18S primers (50 nM at 61°C annealing temperature; Ambion) were used as an internal control for real-time PCR using capillaries (Roche Applied Science), recombinant *Taq* polymerase (Invitrogen), and *Taq* start antibody (Clontech). The primer pairs for the quantitative real-time PCR are listed in Table 1 along with their annealing temperatures, extension times, and base pair yields. Real-time PCR for the listed genes was performed in PCR buffer (20 mM Tris-Cl<sup>–</sup>, pH 8.4, 25°C, and 4 mM MgCl<sub>2</sub>, to which was added 250  $\mu$ g/ml bovine serum albumin and 200  $\mu$ M deoxynucleotides) containing SYBR Green (1:84,000 dilution), 0.05 U/ $\mu$ l *Taq* DNA polymerase, and *Taq* Start antibody (1:100 dilution) as we described previously (31).

**cRNA microarray assay and data analysis.** Total RNA was isolated from 2T3 cells exposed to simulated microgravity and static controls

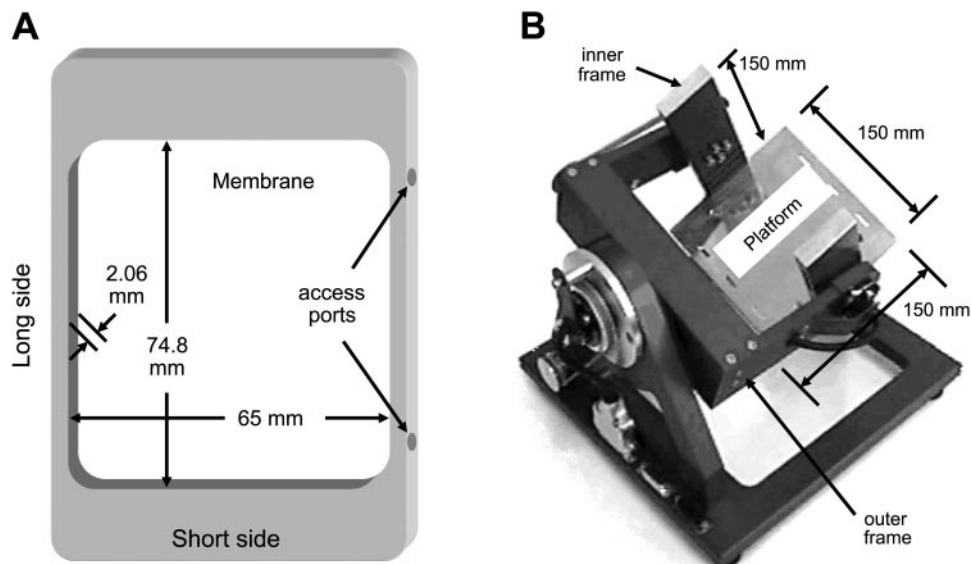


Fig. 1. In vitro simulated microgravity system using 2T3 cells cultured in OptiCell disks and the Random Positioning Machine (RPM). **A:** OptiCell is a sealed cell culture disk formed between two optically clear, gas-permeable polystyrene membranes containing two ports that allow access to the contents. The internal disk dimensions are 74.8  $\times$  65  $\times$  2.06 mm, which can be filled with 10- to 14-ml of medium. **B:** RPM is composed of two motors that independently control the rotation of the outer and inner frames. The total size of the RPM is 30  $\times$  30  $\times$  30 cm, with a functional cargo volume of 150  $\times$  150  $\times$  150 mm. OptiCell disks are mounted at the center of the stainless steel platform attached to the inner frame.

Table 1. Mouse primers used for quantitative real-time RT-PCR

GeneBank Accession No.	Gene	Primers (5'-3')	bp	Conditions for LightCycler	Ref. No.
NM_007431	<i>alp</i>	Forward CAGTATGAATTGAATCGGAACAACC Reverse CAGCAAGAAGAAGCCTTTGAGG	107	7 s at 62°C 6 s at 72°C	25
NM_009820	<i>runx2</i>	Forward GACAGAAGCTTGATGACTCTAAACC Reverse TCTGTAATCTGACTCTGCCTTGT	171	7 s at 62°C 9 s at 72°C	25
NM_011199	<i>pth1r</i>	Forward GCACACAGCAGCCAACATAA Reverse CGCAGCCTAAACGACAGGAA	531	7 s at 63°C 22 s at 72°C	37
NM_012050	<i>omd</i>	Forward GACGGGCTGGTGAATGTGACTATGCTTGA Reverse CCAAGGGGCATTGATTCTAATCTGTTATT	147	7 s at 63°C 10 s at 72°C	
NM_007802	<i>ctsk</i>	Forward AAGTGTTTCCAGAGATGACGGGAC Reverse TCTTCAGAGTCAATGCCTCCGTTC	342	5 s at 55°C 13 s at 72°C	

for 3 days using the RNeasy kit (Qiagen) as described previously. Simulated microgravity and control experiments were performed in triplicate. The samples were reverse transcribed, and the second strand was synthesized using T7 RNA polymerase and biotinylated 2-deoxynucleotide 5'-triphosphate according to the Amersham Biosciences instructions (27). Each cRNA preparation was then hybridized to individual CodeLink Uniset Mouse 1 Bioarrays (Amersham Biosciences) containing synthetic oligonucleotide probes corresponding to 10,000 unique mouse genes in an Amersham Biosciences facility in New Jersey (27). The gene expression intensity was determined using Cy5-streptavidin conjugated to the biotin. The processed slides were scanned using an Axon GenePix Scanner with CodeLink Expression Analysis software (27). The fluorescence intensities of individual probes that were above the threshold levels determined using internal controls were considered to be expressed by the cells and were further analyzed using CodeLink software (Amersham Biosciences). The median intensity of all discovery probes in each microarray was used to normalize the fluorescence intensity of individual gene probes (normalized fluorescence intensity) to minimize interarray variations using CodeLink software. The filtered and normalized data were statistically analyzed using Student's *t*-test, and the genes that changed more than twofold above or below the static 1-g controls with  $P < 0.05$  in response to simulated microgravity were deemed considerable and significant. These genes were plotted using heat map software that we developed. GoMiner software (<http://www.miblab.gatech.edu/gominer/>) was used to sort the genes by biological processes and to assign some of the known functions of each known gene (43).

**Stress and strain analyses.** The attached cells grown on the OptiCell membranes could be exposed to mechanical forces such as fluid shear stress and strain in addition to simulated microgravity during the RPM rotation. To visualize the dynamics of the fluid within the OptiCell, we marked the OptiCell disks with calibrated grids and filled them with water containing colored bead markers (1.018 g/ml density; Amersham Biosciences) with a density close to that of water. Short movies were then recorded using a digital camera mounted on the RPM to track the bead movements over precalibrated grids to estimate flow velocities. The shear stress ( $\tau$ ) was calculated using Newton's law of viscosity as follows:

$$\tau = \mu \left( \frac{v}{h} \right) \quad (1)$$

where  $\mu$  is the viscosity of water and growth medium at 37°C ( $6.92 \times 10^{-4}$  and  $7.8 \times 10^{-4}$  kg·m<sup>-1</sup>·s<sup>-1</sup>, respectively), and  $h$  is half the height of the fluid within the OptiCell (1.028 mm). These calculations suggested that the magnitude of shear stress by growth medium at the membrane level was close to 0 for 43 s, 0.09–0.22 dyn/cm<sup>2</sup> for 13 s, and 0.22–0.44 dyn/cm<sup>2</sup> for 4 s during a 1-min period of random rotation by the RPM. The maximum shear intensity was present at the larger radii of the OptiCell close to the frame, while the center portions of the membranes experienced minimum shear.

Another potential force that cells in the OptiCell disks may experience during the random rotations of the RPM is strain caused by the momentum force of the fluid exerted on the membranes due to sudden directional changes. The strain ( $\epsilon$ ) was calculated using the 1-D wave equation with fixed boundary conditions at both ends of the OptiCell frame. In addition, we assumed that the maximum height of the stretched membrane ( $h$ ) was located at half the membrane length ( $L$ ). The static solution to this wave equation for the first harmonic with the above constraints can be described as follows:

$$f(x) = h \times \sin \left( \frac{\pi x}{2L} \right) \quad (2)$$

where  $f(x)$  is the assumed shape of the membrane when filled with 14 ml of medium,  $h$  is the gap height between the stretched membrane at the center (when filled with medium) and the unstretched membrane (when unfilled), and  $L$  is equal to  $L_{\text{short}}$ , one-half the length of the membrane's short side, and  $L_{\text{long}}$ , one-half the length of the membrane's long side. To determine the length of these arcs, we used the following integral formula:

$$\text{arc} = \int_0^L \sqrt{1 + [f'(x)]^2} dx \quad (3)$$

We calculated the arc for the filled OptiCell when RPM was not rotating, where the height is equal to  $h$ , and then the arc at  $h + \Delta h$ , where  $\Delta h$  is the change in gap height due to additional membrane stretch occurring during sudden directional changes by the RPM rotation. The strain ( $\epsilon$ ) of the membrane along the short and long sides was calculated as follows:

$$\epsilon = \frac{\text{arc}_{h+\Delta h} - \text{arc}_h}{\text{arc}_h} \quad (4)$$

This calculation suggests that maximum microstrain occurs at the center of the longer side of the membrane with a magnitude  $< 200$  microstrains. Although we have not determined the time-dependent changes in the strain, we assume that the maximum strain occurred only briefly during sudden directional changes of the RPM.

**Statistical analysis.** Statistical analysis was performed using Student's *t*-test for all experiments. A significance level of  $P < 0.05$  from three or more independent experiments was considered statistically significant.

## RESULTS

Exposure of 2T3 cells to simulated microgravity using the RPM does not alter cell morphology and proliferation characteristics.



To examine the effects of simulated microgravity on osteoblasts, we developed an *in vitro* system to expose 2T3 cells grown in gas-permeable culture disks (OptiCell) to the RPM. The morphologies of 2T3 cells grown in standard tissue culture dishes and OptiCells were indistinguishable (data not shown). When cells grown in OptiCells were exposed to the simulated microgravity or static 1-g conditions, the pH of the medium remained neutral at or near pH 7.4 (data not shown). As shown in Fig. 2A, the morphologies of 2T3 cells exposed to static 1-g controls and the RPM were not significantly different from each other.

Next, we examined whether RPM exposure induced any changes in 2T3 cell proliferation. For this study, OptiCells were seeded at 2 million cells per disk. Three days later (*day 0* of the experiment), the cell numbers reached  $\sim 3$  million cells per disk (Fig. 2B). The cells were fed with fresh medium every 3 days during the experiment, and they continued to grow to a maximum of  $13 \text{ million} \pm 1.1 \text{ million}$  cells (static 1-g control on *day 7*) and  $10.8 \text{ million} \pm 0.3 \text{ million}$  cells (RPM on *day 7*), showing no statistical difference between the two groups ( $n = 6-7$  experiments;  $P = 0.10$ ). The cell numbers in both groups reached a maximum by *day 5* and remained unchanged until *day 7*. The control group tended to show a variable decrease ( $P > 0.05$ ) in cell numbers by *day 9*. To determine whether these variable decreases in cell numbers were due to increased cell detachment caused by a variety of factors including cell overcrowding or cell death, we counted the number of detached cells in the medium on *day 9* using a Trypan blue assay.

Although the total number of detached cells tended to be higher in the simulated microgravity group ( $194,250 \pm 6,475$ ) than in the static group ( $103,600 \pm 33,645$ ), this difference did not reach statistical significance ( $n = 6$ ;  $P > 0.05$ ). Taken together, these results suggest that simulated microgravity conditions do not have significant effects on cell proliferation within the experimental periods.

*Exposure of 2T3 cells to simulated microgravity inhibits alkaline phosphatase activity.* Because alkaline phosphatase is an established marker for osteoblast differentiation and bone mass formation (39), we chose to determine whether exposing 2T3 cells to simulated microgravity using the RPM would inhibit enzyme activity. As shown in Fig. 3, alkaline phosphatase activity of 2T3 cells increased during culture as expected. The alkaline phosphatase activity of the static-cultured cells dramatically increased more than eightfold within 2 days between *days 1* and 3. By *day 5*, the activity in control cells reached a maximum ( $24 \pm 1 \mu\text{mol} \cdot \text{min}^{-1} \cdot \text{mg}$  of protein $^{-1}$ ), which remained at the maximum at *day 7*. In contrast, exposure of 2T3 cells to the RPM significantly blunted the culture time-dependent increase in alkaline phosphatase activity (Fig. 3). Unlike the static control group, the enzyme activity of the RPM group at *day 3* did not increase significantly above the *day 1* level. By *day 9*, the alkaline phosphatase activity was fourfold that of the *day 1* level. As shown in Fig. 3, the enzyme activity of the static 1-g group was 2.7 times higher than that of the RPM group at *day 9*. This finding that simulated microgravity significantly decreased alkaline phosphatase ac-

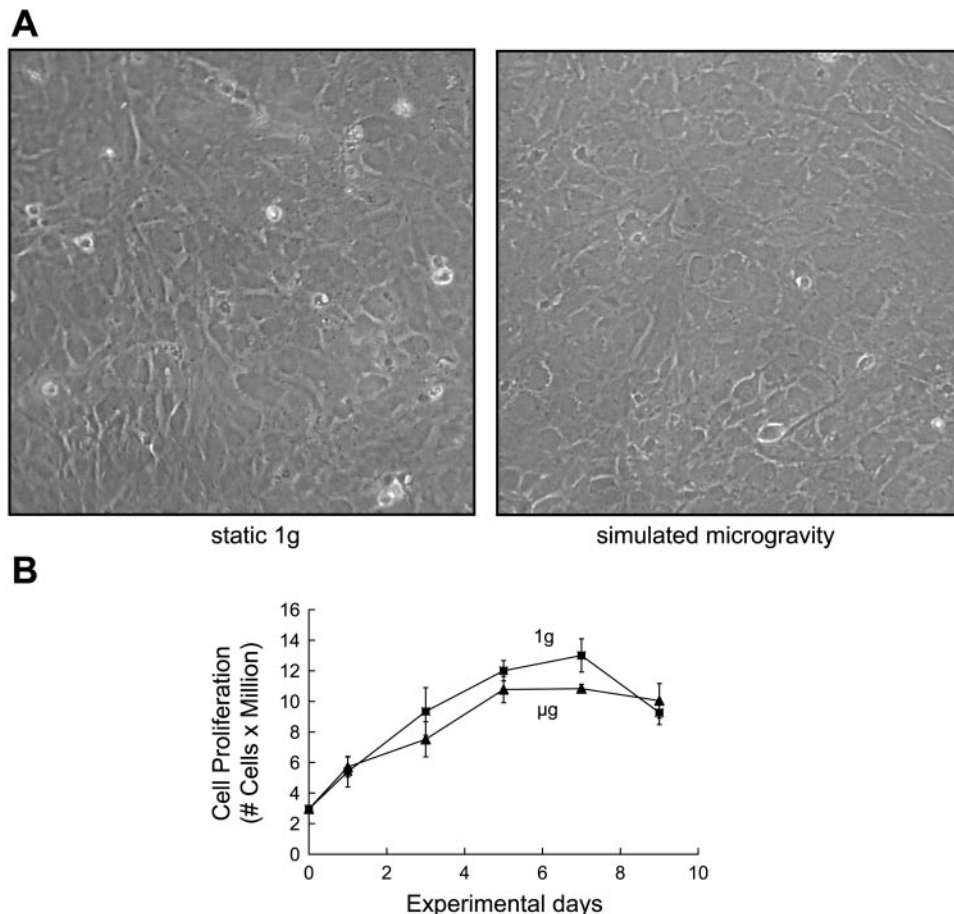


Fig. 2. Simulated microgravity has no significant effect on 2T3 cell morphology and proliferation. On *day 0*, 2T3 cells grown in OptiCells were placed on the RPM or exposed to the static 1-g condition for 1, 3, 5, 7, or 9 days. Cells were fed every 3 days with fresh medium. *A*: representative phase-contrast photomicrograph (original magnification,  $\times 100$ ) of 2T3 cells exposed to either control 1-g condition or RPM for 3 days. *B*: cell proliferation was determined by counting the number of cells in each OptiCell using the Coulter counter as shown in the bar graph (mean  $\pm$  SE;  $n = 6$ ).

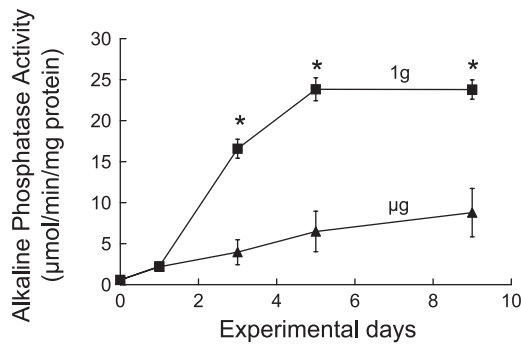


Fig. 3. Simulated microgravity inhibits alkaline phosphatase activity of 2T3 cells. Three days after seeding (*day 0*), 2T3 cells in the OptiCells were placed on the RPM or exposed to the static 1-g condition for 1, 3, 5, or 9 days. The alkaline phosphatase activity in the cell lysate was determined using a colorimetric Sigma assay as described in METHODS. The line graph represents average alkaline phosphatase activity normalized against milligrams of cell lysate proteins. Data are means  $\pm$  SE;  $n = 9$ . \* $P < 0.05$ .

tivity is consistent with the inhibitory effects of microgravity on osteoblast differentiation and bone formation.

*Simulated microgravity altered gene expression profiles of 2T3 cells as determined using microarray studies.* By performing microarray studies, we were able to analyze the global changes in the gene expression profiles of 2T3 cells exposed to simulated microgravity. Among 10,000 gene probes examined with the microarray, only 88 were downregulated and 52 were upregulated to statistically significant levels ( $P < 0.05$ ) more than twofold compared with the static control levels (Fig. 4). Table 2 categorizes genes with known functions from the microarray studies that were upregulated or downregulated significantly ( $P < 0.05$ ) more than twofold above the control. Because these genes were sorted on the basis of typical cell function using the GoMiner program, genes with no known functions were not included in this analysis. Table 3 shows genes from the microarray study that have potential involvement in osteoblast differentiation and matrix mineralization, regardless of the twofold change threshold.

Many osteoblast genes that have been shown to be relevant in bone formation were influenced by simulated microgravity. Alkaline phosphatase, a known marker for bone formation, was downregulated fivefold below the static 1-g control using simulated microgravity. *Runx2*, a transcription factor regulating osteocalcin levels, was downregulated 1.88-fold in microgravity compared with the static 1-g control condition. Parathyroid hormone receptor 1 (*pTHR1*), which acts directly on the skeleton to promote  $Ca^{2+}$  release from bone and on the kidney to enhance  $Ca^{2+}$  reabsorption, was downregulated fivefold by simulated microgravity. On the other hand, inducers of osteolytic activity were also upregulated by simulated microgravity. For example, cathepsin K (*ctsk*) was upregulated 1.66-fold above the static 1-g control. Although the relative changes for *runx2* and *ctsk* fall slightly below the twofold change threshold for significance, we think that both of these genes are potentially important in microgravity-induced genetic changes observed in 2T3 cells because of their established relevance in bone formation and resorption. Thus we also verified the microarray relative changes of these genes using RT-PCR.

These results are consistent with the notion that simulated microgravity decreases the expression of genes necessary for differentiation, matrix formation, and subsequent mineraliza-

tion while increasing the expression of genes that trigger osteoclast activity.

*CodeLink bioarray was verified using quantitative reverse transcriptase real-time PCR.* To verify the results of the microarray studies using real-time PCR, we decided to choose genes that have been shown to be involved in osteoblast differentiation and bone mass regulation. The same samples used for the CodeLink bioarray assays were used for real-time PCR. All real-time PCR data shown in Fig. 5, A–E, were normalized to the internal control, 18S, and the relative changes were determined by dividing the amount of a gene exposed to simulated microgravity by the static 1-g control (Fig. 5F). 2T3 cells exposed to simulated microgravity had decreases in *alp*, *runx2*, *pTHR1*, and osteomodulin (*omd*) gene expression of 0.2, 0.5, 0.2, and 0.2-fold, respectively, as evaluated using the CodeLink bioarray. In addition, 2T3 cells showed an increase in *ctsk* of 1.66-fold. To verify these results, quantitative RT-PCR was performed. While the primers used for *omd* and *ctsk* were designed by us, the other primers used for quantitative real-time PCR were as described in the publications listed in Table 1. The gene expression changes revealed using real-time PCR for *alp*, *runx2*, *pTHR1*, and *omd* were 0.2, 0.7, 0.3, and 0.2-fold, respectively. The change in *ctsk* revealed using RT-PCR was 1.67-fold. In addition, we confirmed the expression of nongravisensitive genes such as bone morphogenic protein 4 (*BMP4*) and cystatin C (*cys C*) using immunoblotting. We show that the changes for *BMP4* and *cys C* determined using Western blot analysis were 1.12- and 1.13-fold, respectively, and that those found using CodeLink were

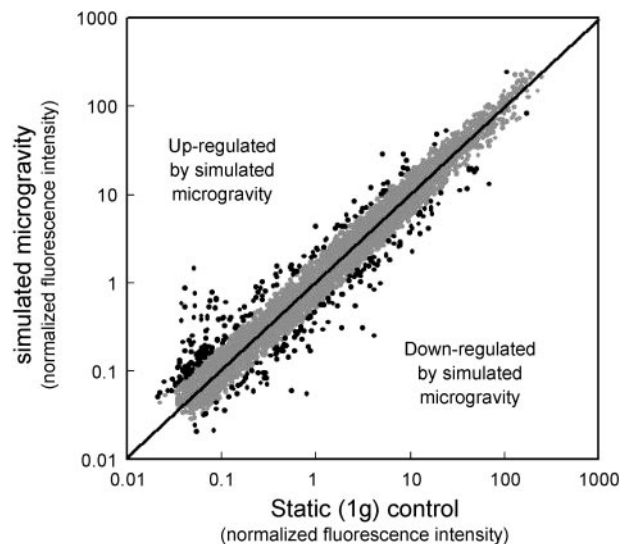


Fig. 4. Overall effects of simulated microgravity on gene expression profiles of 2T3 cells gathered from the microarray analysis. Total RNA was isolated from 2T3 cells exposed to simulated microgravity or static 1-g controls in OptiCells for 3 days as described in Fig. 2. For each sample ( $n = 3$  for microgravity and static 1-g control), cRNA was then synthesized by performing reverse transcription and hybridized to probes on individual CodeLink bioarrays corresponding to 10,000 mouse genes. Statistical analysis identified 140 of 10,000 genes that changed more than twofold above or below static 1-g control ( $P < 0.05$ ). Scatterplot shows mean intensities of each gene probe using data obtained from all microarrays ( $n = 3$ , simulated microgravity and static 1-g control). Genes changed by simulated microgravity more than twofold above or below static 1-g levels are shown as solid dots, while all others are shown as shaded dots. The full data set is available at the NCBI-GEO web site (accession no. GDS 928).

Table 2. Selected genes sensitive to simulated microgravity in 2T3 cells sorted on the basis of typical cell functions

GenBank Accession No.	Gene	Fold Change	SE	P Value	Molecular Function
<b>Cell adhesion</b>					
NM_012050	<i>Osteomodulin</i>	0.184	±0.031	<0.01	A/k/a osteoadherin; may mediate cell attachment
AF064749	<i>Collagen, type VI, α<sub>3</sub></i>	0.213	±0.012	<0.05	Extracellular matrix structural constituent
NM_007729	<i>Procollagen, type XI, α<sub>1</sub></i>	0.292	±0.013	<0.025	Extracellular matrix structural constituent
NM_008462	<i>Killer cell lectin-like receptor, subfamily A, member 2</i>	2.202	±0.311	<0.05	Binding and signal transducer activity
<b>Cell cycle</b>					
NM_011817	<i>Growth arrest and DNA damage-inducible-γ (GADD45G)</i>	0.485	±0.081	<0.025	Structural constituent of ribosome
NM_021515	<i>Adenylate kinase 1</i>	0.490	±0.042	<0.025	Nucleobase, nucleoside, nucleotide kinase activity
NM_008654	<i>Myeloid differentiation primary response gene 116 (MYD116)</i>	2.004	±0.187	<0.025	Myeloid differentiation primary response gene induced by IL-6
NM_007836	<i>Growth arrest and DNA damage-inducible 45 α (GADD45A)</i>	2.405	±0.193	<0.025	Structural constituent of ribosome
<b>Development</b>					
NM_009964	<i>Crystalline, αB</i>	0.351	±0.061	<0.05	Chaperone and heat shock protein activity
NM_009144	<i>Secreted frizzled-related sequence protein 2</i>	0.409	±0.009	<0.005	Transmembrane receptor and signal transduction activity
<b>Metabolism</b>					
NM_007431	<i>Alkaline phosphatase 2, liver</i>	0.210	±0.017	<0.01	Essential for hydroxyapatite formation and matrix mineralization
NM_008196	<i>Granzyme K</i>	0.279	±0.014	<0.025	Hydrolase and peptidase activity
M58755	<i>Glucokinase</i>	0.318	±0.017	<0.01	Hexokinase activity
NM_009128	<i>Stearoyl-coenzyme A desaturase 2</i>	0.347	±0.050	<0.01	Metal ion binding and oxidoreductase activity
NM_007934	<i>Glutamyl aminopeptidase</i>	0.350	±0.042	<0.005	Metalloexopeptidase activity
NM_010941	<i>NAD(P)-dependent steroid dehydrogenase-like</i>	0.367	±0.021	<0.025	Oxidoreductase activity, acting on CH-OH group of donors
NM_015744	<i>Ectonucleotide pyrophosphatase/phosphodiesterase 2</i>	0.376	±0.087	<0.025	Hydrolase activity
NM_010255	<i>Guanidinoacetate methyl transferase</i>	0.406	±0.069	<0.05	Methyltransferase activity
NM_018887	<i>Cytochrome P450, 39A1</i>	0.435	±0.051	<0.05	Oxidoreductase activity
NM_008976	<i>Protein tyrosine phosphatase, nonreceptor type 14</i>	0.451	±0.034	<0.01	Phosphoric monoester hydrolase activity
NM_020010	<i>Cytochrome P450, 51</i>	0.486	±0.011	<0.025	Oxidoreductase activity
NM_019425	<i>Glucosamine-phosphate N-acetyltransferase 1</i>	2.041	±0.077	<0.01	Transferase activity
NM_012006	<i>Cytosolic acyl-CoA thioesterase 1</i>	2.165	±0.175	<0.025	CoA hydrolase activity
NM_033320	<i>Glucuronyl c5 epimerase</i>	2.184	±0.105	<0.025	Racemase and epimerase activity on carbohydrates
NM_007703	<i>Cig30 or (FEN1/ELO2, SUR4/ELO3, yeast)-like 3 (ELOVL3)</i>	2.377	±0.157	<0.025	Involved in a pathway connected with brown fat hyperplasia
NM_009943	<i>Cytochrome c oxidase, subunit VI A, polypeptide 2</i>	2.669	±0.199	<0.01	Oxidoreductase activity on heme group of donors
NM_007823	<i>Cytochrome P450, subfamily IV B, polypeptide 1</i>	3.925	±0.241	<0.005	Oxidoreductase activity
NM_009802	<i>Carbonic anhydrase 6</i>	5.571	±1.077	<0.05	Carbon-oxygen lyase and hydrolyase activity
<b>Protein metabolism</b>					
NM_010222	<i>FK506 binding protein 7</i>	0.485	0.073	<0.05	Peptidyl-prolyl <i>cis-trans</i> -isomerase activity
NM_011985	<i>Matrix metalloproteinase 23</i>	0.493	0.009	<0.025	Metalloendopeptidase activity
NM_011710	<i>Tryptophanyl-TRNA synthetase</i>	2.080	0.085	<0.025	Ligase activity, forming phosphoric ester and carbon-oxygen bonds
NM_011361	<i>Serum/glucocorticoid-regulated kinase</i>	2.169	0.014	<0.005	Serine/threonine kinase activity
NM_015774	<i>ERO1-like</i>	2.305	0.108	<0.01	Unknown
NM_011670	<i>Ubiquitin carboxy-terminal hydrolase L1</i>	2.354	0.423	<0.05	Thiolester hydrolase activity
<b>Stress or immune response</b>					
NM_010357	<i>Glutathione S-transferase, α<sub>4</sub></i>	0.368	0.046	<0.05	Transferase activity, transferring alkyl or aryl groups
NM_008599	<i>Small inducible cytokine B subfamily, member 9</i>	0.430	0.069	<0.025	G protein-coupled receptor binding activity
NM_010358	<i>Glutathione-S-transferase, μ<sub>1</sub></i>	0.482	0.085	<0.05	Transferase activity, transferring alkyl or aryl groups
AF321817	<i>LPTS1</i>	2.001	0.293	<0.05	Nucleic acid binding activity
NM_009635	<i>Advillin</i>	2.588	0.308	<0.025	Structural constituent of cytoskeleton
<b>Sensory perception</b>					
NM_009073	<i>Rod outer segment membrane protein 1 (ROM1)</i>	0.390	0.172	<0.05	G protein-coupled photoreceptor activity



Table 2.—Continued

GenBank Accession No.	Gene	Fold Change	SE	P Value	Molecular Function
Signal transduction					
NM_011338	<i>Small inducible cytokine A9</i>	0.287	0.046	<0.005	G protein-coupled receptor binding activity
NM_013641	<i>Prostaglandin E receptor 1</i>	0.338	0.026	<0.005	Transmembrane and G protein-coupled receptor activity
AB040819	<i>RAC3</i>	0.377	0.012	<0.05	GTPase activity
NM_011058	<i>Platelet-derived growth factor receptor, <math>\alpha</math>-polypeptide</i>	0.378	0.025	<0.025	Transmembrane receptor protein tyrosine kinase activity
NM_010315	<i>Guanine nucleotide binding protein, <math>\gamma</math>-subunit</i>	0.404	0.041	<0.05	Heterotrimeric G protein GTPase activity
NM_016894	<i>RAMP1</i>	0.418	0.047	<0.025	Coreceptor, soluble ligand activity
NM_009138	<i>Small inducible cytokine A25</i>	2.038	0.117	<0.01	G protein-coupled receptor binding activity
NM_008519	<i>Leukotriene B4 receptor</i>	2.276	0.092	<0.025	Rhodopsin-like transmembrane receptor activity
Skeletal development					
NM_011199	<i>Parathyroid hormone receptor</i>	0.198	0.010	<0.005	Transmembrane receptor activity
NM_011606	<i>Tetranectin</i>	0.187	0.027	<0.025	Binds to plasminogen; may regulate matrix mineralization
NM_054077	<i>Proline arginine-rich end leucine-rich repeat</i>	0.453	0.037	<0.005	Extracellular matrix structural constituent
Transcription					
NM_010753	<i>Max dimerization protein 4 (MAD4)</i>	0.261	0.058	<0.025	Transcription regulator activity
NM_010497	<i>Isocitrate dehydrogenase 1 (NAP+), soluble</i>	0.409	0.094	<0.025	Oxidoreductase activity on CH-OH group of donors
NM_010235	<i>FOS-like antigen 1</i>	2.328	0.199	<0.025	DNA binding activity
NM_016660	<i>High-mobility group protein 1</i>	3.060	0.442	<0.025	DNA binding activity

1.03- and 0.71-fold, respectively (Fig. 5G). The different methodologies used (real-time PCR, immunoblotting, and microarray assay) produced highly consistent results, providing a level of assurance regarding the validity of the microarray data.

## DISCUSSION

The novel and most significant finding of the current study is that exposure of preosteoblasts to simulated microgravity using the RPM recapitulates some of the expected changes associated with the bone loss response observed in spaceflight. As expected in spaceflight microgravity conditions, simulated microgravity induced a loss of alkaline phosphatase mRNA and activity, a marker of differentiation. We also found that this change occurred without altering the cell proliferation and gross morphology of 2T3 cells. Using this *in vitro* system, the current study generated a list of genes that are upregulated, downregulated, or unchanged by simulated microgravity. Several genes that are suspected to be involved in bone formation and loss have been found to change in the expected manner. We selected seven genes (*alp*, *runx2*, *pthr1*, *omd*, *ctsk*, *BMP4*, and *cys C*) from the list and verified the microarray results using real-time PCR or Western blot analysis.

Microgravity-induced bone loss in humans and animals has been shown to be mediated at least in part by osteoblast differentiation, and alkaline phosphatase is a well-known marker for it (3, 6, 20). Our finding that 2T3 cell exposure to the RPM decreased *alp* and *runx2* expression is consistent with the spaceflight data obtained with osteoblasts as well as with other simulated microgravity data using cultured calvaria, human mesenchymal stem cells, and MC3T3-E1 cells exposed to a rotating wall vessel (5, 7, 25, 42). The decrease in alkaline phosphatase activity could be used as an indicator of space-

flight-induced inhibition of preosteoblast differentiation to osteoblasts, leading to bone loss (10). The *runx2* gene, a member of the runt homology domain transcription factor family, which regulates osteocalcin, is an essential transcription factor for osteoblast differentiation and bone formation. We found that *runx2* was downregulated almost twofold below the static 1-g control. Osteocalcin protein levels in conditioned medium, however, were too low to be detected in our studies because of a relatively short experimental duration of up to 9 days, and this finding is consistent with the findings described in a previous report (11). On the other hand, osteocalcin level was shown to be decreased by exposure to rotating wall vessel in mouse calvaria and a different osteoblast cell line, MC3T3-E1 (25, 42). Osteomodulin belongs to a small, leucine-rich proteoglycan family and is involved in bone matrix formation (4). Our present study showing the downregulation of osteomodulin by simulated microgravity supports our hypothesis. The decrease in parathyroid hormone-related protein, which plays a role in  $\text{Ca}^{2+}$  mobilization, has been linked to the decrease in bone density and bone loss in rats during spaceflight (32). In this light, our result demonstrating that PTH receptor 1 mRNA levels decrease by simulated microgravity is also consistent with the spaceflight data. In addition to the downregulated genes, several genes and proteins were upregulated. Cathepsin K, which is a member of the papain family of cysteine proteases, is expressed mostly in osteoclasts and plays a critical role in bone resorption (22, 41). More recently, however, cathepsin K has been found in nonosteoclastic cells such as thyroid epithelial cells (41). As far as we know, our present study represents the first time that cathepsin K expression has been found in osteoblasts. At present, the biological and pathophysiological implications of cathepsin K expression in

Table 3. Effect of microgravity on selected genes that may be involved in osteoblast differentiation and matrix mineralization, sorted on the basis of fold changes

GenBank Accession No.	Gene	Fold $\Delta$	SE	P Value	Molecular Function
NM_012050	<i>Osteomodulin</i>	0.184	$\pm 0.031$	<0.01	A/k/a osteoadherin; may mediate cell attachment
NM_011606	<i>Tetranectin</i>	0.187	$\pm 0.027$	<0.025	Binds to plasminogen; may regulate matrix mineralization
NM_011199	<i>Parathyroid hormone receptor</i>	0.198	$\pm 0.010$	<0.005	Transmembrane receptor activity
NM_007431	<i>Alkaline phosphatase 2, liver</i>	0.210	$\pm 0.017$	<0.01	Essential for hydroxyapatite formation and matrix mineralization
NM_008524	<i>Lumican</i>	0.259	$\pm 0.030$	<0.005	Regulates collagen fibril formation in different extracellular matrices
NM_007729	<i>Procollagen, type XI, <math>\alpha_1</math></i>	0.292	$\pm 0.013$	<0.025	Present in cartilage
NM_007559	<i>Bone morphogenetic protein 8B</i>	0.337	$\pm 0.071$	<0.1	Growth factor and cytokine activity
NM_008760	<i>Osteoglycin</i>	0.380	$\pm 0.003$	<0.025	Binds to TGF- $\beta$ , no GAG in bone, keratan sulfate in other tissues
NM_016894	<i>RAMP1</i>	0.418	$\pm 0.047$	<0.025	Calcitonin signal transducer activity
NM_007743	<i>Procollagen, type I, <math>\alpha_2</math></i>	0.431	$\pm 0.091$	<0.1	Major constituent of bone matrix
NM_021355	<i>Fibromodulin</i>	0.450	$\pm 0.103$	<0.1	Binds to collagen; may regulate fibril formation; binds to TGF- $\beta$
NM_019444	<i>RAMP2</i>	0.500	$\pm 0.027$	<0.005	Calcitonin signal transducer activity
AF053954	<i>cbfa1/runx2 (osf2)</i>	0.533	$\pm 0.058$	<0.1	Essential transcription factor for osteoblast differentiation and bone formation
NM_007833	<i>Decorin</i>	0.562	$\pm 0.003$	<0.005	Binds to collagen; may regulate fibril diameter
NM_013691	<i>Thrombospondin 3</i>	0.581	$\pm 0.034$	<0.01	Involved in cell attachment
NM_011607	<i>Tenascin C</i>	0.589	$\pm 0.024$	<0.025	Noncollagenous macromolecule of cartilage matrix
NM_011693	<i>Vascular cell adhesion molecule 1</i>	0.633	$\pm 0.075$	<0.05	Cell adhesion molecule activity
NM_008970	<i>Parathyroid hormone-like peptide</i>	0.655	$\pm 0.233$	>0.1	Signal transduction and hormone activity
NM_007553	<i>Bone morphogenetic protein 2</i>	0.704	$\pm 0.065$	<0.05	Growth factor and cytokine activity
NM_016919	<i>Procollagen, type V, <math>\alpha_3</math></i>	0.716	$\pm 0.024$	<0.1	Present where there is collagen type I
NM_011581	<i>Thrombospondin 2</i>	0.724	$\pm 0.298$	>0.1	Involved in cell attachment
NM_013605	<i>Mucin 1</i>	0.733	$\pm 0.047$	<0.05	Cell adhesion receptor
NM_011146	<i>Peroxisome proliferator activated receptor-<math>\gamma</math></i>	0.734	$\pm 0.016$	<0.1	RNA polymerase II transcription factor
NM_007433	<i>Alkaline phosphatase 5</i>	0.736	$\pm 0.108$	>0.1	Hydrolase activity on ester bonds
NM_010514	<i>Insulin-like growth factor 2</i>	0.752	$\pm 0.077$	<0.1	Signal transduction and hormone activity
NM_007737	<i>Procollagen, type V, <math>\alpha_2</math></i>	0.767	$\pm 0.026$	<0.1	Present where there is collagen type I
NM_022415	<i>Prostaglandin E synthase</i>	0.778	$\pm 0.041$	<0.05	Intramolecular isomerase activity, other intramolecular oxidoreductases
NM_010512	<i>Insulin-like growth factor 1</i>	0.785	$\pm 0.190$	>0.1	Signal transduction and hormone activity
NM_007644	<i>CD36 antigen-like 2</i>	0.833	$\pm 0.013$	<0.025	Signal transducer activity
NM_010181	<i>Fibrillin 2</i>	0.842	$\pm 0.172$	>0.1	May regulate elastic fiber formation (calcium ion binding activity)
NM_013731	<i>Serum/glucocorticoid-regulated kinase 2</i>	0.848	$\pm 0.348$	>0.1	Phosphotransferase activity, alcohol group as acceptor
NM_009262	<i>Osteonectin (SPOCK1)</i>	0.853	$\pm 0.210$	>0.1	May mediate deposition of hydroxyapatite, binds to growth factors
NM_011707	<i>Vitronectin</i>	0.861	$\pm 0.297$	>0.1	Binds to collagen, plasminogen, and heparin
NM_008712	<i>Nitric oxide synthase 1</i>	0.861	$\pm 0.025$	<0.1	Nitric oxide synthase activity
L27439	<i>Protein S</i>	0.864	$\pm 0.170$	>0.1	Calcium ion binding activity
NM_008689	<i>NP-<math>\kappa</math>B 1</i>	0.875	$\pm 0.027$	<0.05	Transcription factor activity
NM_011808	<i>ETS 1</i>	0.883	$\pm 0.199$	>0.1	Transcription factor expressed in proliferating preosteoblastic cells
NM_007388	<i>Acid phosphatase 5, tartrate-resistant</i>	0.885	$\pm 0.180$	>0.1	Enzyme identified in the ruffled border of the osteoclast membrane
NM_011519	<i>Syndecan 1</i>	0.890	$\pm 0.047$	>0.1	Binds to type I collagen, fibronectin, tenascin C
NM_007557	<i>Bone morphogenetic protein 7</i>	0.905	$\pm 0.063$	>0.1	Growth factor and cytokine activity
NM_009926	<i>Procollagen, type XI, <math>\alpha_2</math></i>	0.913	$\pm 0.121$	>0.1	Present in cartilage
NM_011347	<i>Platelet selectin</i>	0.920	$\pm 0.075$	>0.1	Cell adhesion molecule activity
NM_007542	<i>Biglycan</i>	0.920	$\pm 0.024$	>0.1	May bind to collagen, a genetic determinant of peak bone mass
M28621	<i>Interferon-<math>\gamma</math></i>	0.945	$\pm 0.161$	>0.1	Inhibits bone resorption
NM_031163	<i>Procollagen, type II, <math>\alpha_1</math></i>	0.947	$\pm 0.171$	>0.1	Major constituent of cartilage
NM_008318	<i>Integrin binding sialoprotein</i>	0.953	$\pm 0.151$	>0.1	Noncollagenous protein in bone
NM_013712	<i>Integrin <math>\beta_1</math> binding protein 2</i>	0.956	$\pm 0.062$	>0.1	Muscle-specific integrin $\beta_1$ -interacting protein
NM_031168	<i>Interleukin-6</i>	0.964	$\pm 0.065$	>0.1	Act as stimulators of an early stage of osteoclast formation
NM_008355	<i>Interleukin-13</i>	0.966	$\pm 0.345$	>0.1	Inhibit bone resorption
NM_020273	<i>Glucocorticoid-modulatory element binding protein 1</i>	0.979	$\pm 0.077$	>0.1	Transcription factor activity
NM_007412	<i>Adrenomedullin receptor</i>	0.981	$\pm 0.125$	>0.1	Rhodopsin-like, G protein-coupled receptor activity
NM_011346	<i>Lymphocyte selectin</i>	0.982	$\pm 0.075$	>0.1	Cell adhesion molecule activity
NM_009367	<i>Transforming growth factor-<math>\beta_2</math></i>	1.000	$\pm 0.127$	>0.1	Growth factor and cytokine activity
NM_009758	<i>Bone morphogenetic protein receptor 1A</i>	1.011	$\pm 0.176$	>0.1	TGF- $\beta$ and BMP receptor
NM_007560	<i>Bone morphogenetic protein receptor 1B</i>	1.024	$\pm 0.144$	>0.1	TGF- $\beta$ and BMP receptor
NM_008713	<i>Nitric oxide synthase 3</i>	1.026	$\pm 0.151$	>0.1	Nitric oxide synthase activity
NM_007424	<i>Aggrecan 1</i>	1.026	$\pm 0.077$	>0.1	Glycosaminoglycan binding activity
NM_007554	<i>Bone morphogenetic protein 4</i>	1.027	$\pm 0.017$	>0.1	Growth factor and cytokine activity
NM_007558	<i>Bone morphogenetic protein 8A</i>	1.049	$\pm 0.186$	>0.1	Growth factor and cytokine activity



Table 3.—Continued

GenBank Accession No.	Gene	Fold $\Delta$	SE	P Value	Molecular Function
NM_007993	<i>Fibrillin 1</i>	1.049	$\pm 0.045$	>0.1	May regulate elastic fiber formation
NM_011809	<i>ETS 2</i>	1.078	$\pm 0.176$	>0.1	Transcription factor expressed in differentiating and mature osteoblasts
NM_010927	<i>Nitric oxide synthase 2</i>	1.086	$\pm 0.195$	>0.1	Nitric oxide synthase activity
NM_011196	<i>Prostaglandin E receptor 3</i>	1.102	$\pm 0.397$	>0.1	Rhodopsin-like, G protein-coupled receptor activity
NM_007643	<i>CD36 antigen</i>	1.102	$\pm 0.461$	>0.1	Cell adhesion molecule activity
NM_008216	<i>Hyaluronan synthase 2</i>	1.116	$\pm 0.240$	>0.1	With versican-like protein, works to capture space destined to become bone
NM_008764	<i>Osteoprotegerin</i>	1.127	$\pm 0.260$	>0.1	Signal transducer activity
NM_008319	<i>Intracellular adhesion molecule 5</i>	1.136	$\pm 0.082$	>0.1	Cell adhesion molecule activity
X97991	<i>Calcitonin</i>	1.149	$\pm 0.096$	>0.1	Signal transducer activity
NM_010735	<i>Lymphotoxin A</i>	1.149	$\pm 0.129$	>0.1	Tumor necrosis factor receptor ligand activity
NM_052994	<i>Osteonectin (SPOCK2)</i>	1.164	$\pm 0.105$	>0.1	May mediate deposition of hydroxyapatite, binds to growth factors
NM_019511	<i>RAMP3</i>	1.172	$\pm 0.042$	>0.1	Calcitonin signal transducer activity
NM_008215	<i>Hyaluronan synthase 1</i>	1.177	$\pm 0.258$	>0.1	With versican-like protein, works to capture space destined to become bone
NM_013693	<i>Tumor necrosis factor</i>	1.256	$\pm 0.334$	>0.1	Growth factor and cytokine activity
NM_010577	<i>Integrin-<math>\alpha</math>5</i>	1.304	$\pm 0.251$	>0.1	Cell adhesion molecule
NM_008350	<i>Interleukin 11</i>	1.312	$\pm 0.379$	>0.1	Act as stimulators of an early stage of osteoclast formation
NM_008518	<i>Lymphotoxin B</i>	1.330	$\pm 0.031$	<0.025	Tumor necrosis factor receptor ligand activity
NM_007761	<i>Calcitonin gene-related peptide receptor</i>	1.345	$\pm 0.102$	<0.1	Calcitonin receptor activity
NM_007588	<i>Calcitonin receptor</i>	1.345	$\pm 0.225$	>0.1	Calcitonin G protein-coupled receptor activity
NM_008217	<i>Hyaluronan synthase 3</i>	1.357	$\pm 0.198$	>0.1	With versican-like protein, works to capture space destined to become bone
NM_010494	<i>Intracellular adhesion molecule 2</i>	1.362	$\pm 0.550$	>0.1	Cell adhesion molecule activity
NM_010576	<i>Integrin-<math>\alpha</math>4</i>	1.413	$\pm 0.448$	>0.1	Cell adhesion molecule
NM_018782	<i>Calcitonin receptor-like</i>	1.413	$\pm 0.242$	>0.1	Calcitonin G protein-coupled receptor activity
NM_011580	<i>Thrombospondin 1</i>	1.418	$\pm 0.278$	>0.1	Cell attachment
NM_009627	<i>Adrenomedullin</i>	1.426	$\pm 0.176$	<0.1	Neuropeptide hormone activity
NM_008965	<i>Prostaglandin E receptor 4</i>	1.445	$\pm 0.581$	>0.1	G protein-coupled receptor activity
NM_008396	<i>Integrin-<math>\alpha</math>2</i>	1.654	$\pm 0.467$	>0.1	Cell adhesion molecule
NM_007802	<i>Cathepsin K (ctsk)</i>	1.661	$\pm 0.076$	<0.01	In the papain family of cysteine proteases
NM_010554	<i>Interleukin-1<math>\alpha</math></i>	1.875	$\pm 0.224$	<0.1	Potent stimulators of bone resorption
NM_007556	<i>Bone morphogenetic protein 6</i>	1.877	$\pm 0.161$	<0.1	Growth factor and cytokine activity
NM_008361	<i>Interleukin-1<math>\beta</math></i>	2.099	$\pm 0.176$	<0.025	Potent stimulators of bone resorption
NM_011361	<i>Serum/glucocorticoid-regulated kinase</i>	2.169	$\pm 0.014$	<0.001	Transferase activity, transferring phosphorus-containing groups
NM_054084	<i>Calcitonin-related polypeptide-<math>\beta</math></i>	9.548	$\pm 8.524$	>0.1	Signal transducer activity

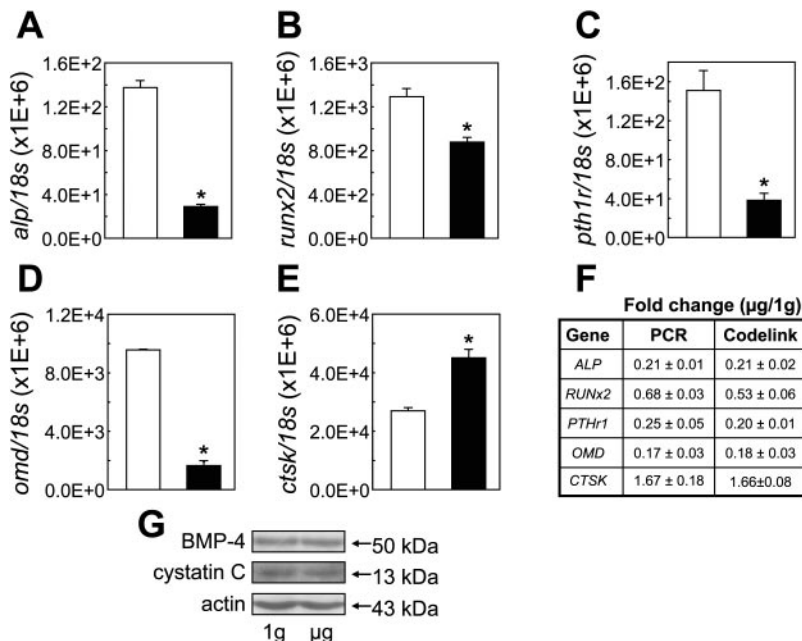


Fig. 5. Microarray results were verified using real-time PCR for genes that were upregulated or downregulated in response to simulated microgravity and using Western blot analysis for genes that did not change. Aliquots of total RNA used for microarray studies ( $n = 3$ , simulated microgravity and static 1-g control) shown in Fig. 4 were used in quantitative real-time PCR assays for five selected genes. Additional sets of total RNA that were obtained from other microgravity and control experiments were used in this study. A–E: mRNA copy numbers of alkaline phosphatase (*alp*), runt-related transcription factor 2 (*runx2*), parathyroid hormone 1 receptor (*pthr1*), osteomodulin (*omd*), and cathepsin K (*ctsk*) were quantified from standard curves using the known amount of corresponding murine cDNA as well as the amount of 18S rRNA. Error bars represent means  $\pm$  SE;  $n = 4$ –6. \* $P < 0.05$ . F: comparison of the CodeLink bioarray fold changes with the quantitative RT-PCR results. G: whole cell lysate obtained from simulated microgravity and static 1-g experiments described in Fig. 4 were used for Western blot analysis with antibodies to bone morphogenetic protein 4 (*BMP4*), cystatin C (*cysC*), and actin. Blot shown is representative of three independent studies.

osteoblasts are not clear. Cathepsin K induced by simulated microgravity could be responsible for bone loss either by directly increasing osteoclastic activity or through an indirect osteoblast-dependent mechanism.

We also examined some genes that were not shown to change in response to simulated microgravity according to the microarray data. For example, *BMP-4* and *cys C* mRNA levels in the RPM-exposed group showed 1.0- and 0.7-fold changes, respectively, over the controls. We performed Western blot analysis to examine their protein expression levels with specific antibodies to *BMP-4*, *cys C*, and actin (as a control) using lysates obtained from 2T3 cells exposed to 3 days of simulated microgravity or static 1-g control conditions. As expected, we did not find any significant difference in their protein expression levels (Fig. 5).

In addition to simulated microgravity, cells in our in vitro system showed a low level of shear stress and strain on the basis of our computational modeling studies. Our model predicts a minor portion of the cells close to the long frames of the OptiCell disk showing significantly less than 1 dyn/cm<sup>2</sup> of shear stress for a brief moment (<4 s/min) and <200 microstrains of mechanical strain for a fraction of the duration of the RPM's rotation. However, the levels of these forces are significantly lower than the reported force magnitudes (as low as 2 dyn/cm<sup>2</sup> shear stress and 500 microstrains) needed to stimulate signaling in osteoblasts (16, 17, 21, 28). However, it also was shown that as low as 0.14 dyn/cm<sup>2</sup> of continuous shear exposure for 4 h increased cyclooxygenase 2 expression (35). Therefore, our results need to be interpreted with the caution that at least some of the observed RPM effects may be due to mechanical forces other than simulated microgravity.

In summary, we have developed a novel in vitro system using RPM and OptiCell disks with 2T3 cells, which seemed to recapitulate the bone loss-like response under microgravity conditions during spaceflight. Our data show that exposure to simulated microgravity changed gene expression profiles and the inhibition of differentiation of preosteoblasts to osteoblasts, eventually leading to reduced bone formation. At this point, whether these two events, differentiation and gene expression change, occur in sequence or concurrently is not clear. It is likely, however, these two events are closely interrelated. In addition to tabulating known and expected genes (e.g., *alp*, *runx2*, *omd*, *pthr1*, and *ctsk*), we have developed a list of unknown and uncharacterized genes that dramatically changed after exposure of 2T3 cells to simulated microgravity. The functional characterization of these expected and unexpected genes will provide critical insight into understanding the mechanisms of microgravity-induced bone loss. Moreover, these studies may lead to the identification of the novel targets of therapeutic interventions to prevent or to cure bone loss in astronauts as well as in the general patient population with metabolic bone diseases.

#### ACKNOWLEDGMENTS

We thank Erik Levy of Amersham Biosciences for work performed on the CodeLink bioarray and Dr. Xu Cao of the University of Alabama at Birmingham for 2T3 cells. We also thank Drs. Barbara Boyan at the Georgia Institute of Technology and Janet Rubin at Emory University for helpful comments as well as Ronald Huijser, Frans Hommes, and Luc van den Bergh at Fokker Science for providing the RPM used during this study.

#### GRANTS

This work was supported by National Aeronautics and Space Administration Grant NAG2-1348 (to H. Jo) and National Heart, Lung, and Blood Institute Grants HL-71014 and HL-67413 (to H. Jo).

#### REFERENCES

1. Al Ajmi N, Braidman IP, and Moore D. Effect of clinostat rotation on differentiation of embryonic bone in vitro. *Adv Space Res* 17: 189–192, 1996.
2. Arbeille P, Fomina G, Achaibou F, Pottier J, and Kotovskaya A. Cardiac and vascular adaptation to 0g with and without thigh cuffs (Antares 14 and Altair 21 day Mir spaceflights). *Acta Astronaut* 36: 753–762, 1995.
3. Bikle DD and Halloran BP. The response of bone to unloading. *J Bone Miner Metab* 17: 233–244, 1999.
4. Buchaille R, Couble ML, Magloire H, and Bleicher F. Expression of the small leucine-rich proteoglycan osteoadherin/osteomodulin in human dental pulp and developing rat teeth. *Bone* 27: 265–270, 2000.
5. Caillot-Augusseau A, Lafage-Proust MH, Soler C, Pernod J, Dubois F, and Alexandre C. Bone formation and resorption biological markers in cosmonauts during and after a 180-day space flight (Euromir 95). *Clin Chem* 44: 578–585, 1998.
6. Caillot-Augusseau A, Vico L, Heer M, Voroviev D, Souberbielle JC, Zitterman A, Alexandre C, and Lafage-Proust MH. Space flight is associated with rapid decreases of undercarboxylated osteocalcin and increases of markers of bone resorption without changes in their circadian variation: observations in two cosmonauts. *Clin Chem* 46: 1136–1143, 2000.
7. Carmeliet G and Bouillon R. The effect of microgravity on morphology and gene expression of osteoblasts in vitro. *FASEB J* 13, Suppl: S129–S134, 1999.
8. Carmeliet G, Vico L, and Bouillon R. Space flight: a challenge for normal bone homeostasis. *Crit Rev Eukaryot Gene Expr* 11: 131–144, 2001.
9. Collet P, Uebelhart D, Vico L, Moro L, Hartmann D, Roth M, and Alexandre C. Effects of 1- and 6-month spaceflight on bone mass and biochemistry in two humans. *Bone* 20: 547–551, 1997.
10. Garetto LP, Gonsalves MR, Morey ER, Durnova G, and Roberts WE. Preosteoblast production 55 hours after a 12.5-day spaceflight on Cosmos 1887. *FASEB J* 4: 24–28, 1990.
11. Ghosh-Choudhury N, Windle JJ, Koop BA, Harris MA, Guerrero DL, Wozney JM, Mundy GR, and Harris SE. Immortalized murine osteoblasts derived from BMP 2-T-antigen expressing transgenic mice. *Endocrinology* 137: 331–339, 1996.
12. Heer M, Kamps N, Biener C, Korrr C, Boerger A, Zittermann A, Stehle P, and Drummer C. Calcium metabolism in microgravity. *Eur J Med Res* 4: 357–360, 1999.
13. Hejnowicz Z, Sondag C, Alt W, and Sievers A. Temporal course of graviperception in intermittently stimulated cress roots. *Plant Cell Environ* 21: 1293–1300, 1998.
14. Hughes-Fulford M. Signal transduction and mechanical stress. *Sci STKE* 2004: RE12, 2004.
15. Huijser RH. Desktop RPM: new small size microgravity simulator for the bioscience laboratory (FS-MG-R00-017). Leiden, The Netherlands: Fokker Space, 2000.
16. Kapur S, Baylink DJ, and Lau KHW. Fluid flow shear stress stimulates human osteoblast proliferation and differentiation through multiple interacting and competing signal transduction pathways. *Bone* 32: 241–251, 2003.
17. Kaspar D, Seidl W, Neidlinger-Wilke C, Ignatius A, and Claes L. Dynamic cell stretching increases human osteoblast proliferation and C1CP synthesis but decreases osteocalcin synthesis and alkaline phosphatase activity. *J Biomech* 33: 45–51, 2000.
18. Katkovsky BS and Pomyotov YD. Cardiac output during physical exercises following real and simulated space flight. *Life Sci Space Res* 14: 301–305, 1976.
19. Kobayashi K, Kambe F, Kurokouchi K, Sakai T, Ishiguro N, Iwata H, Koga K, Gruener R, and Seo H. TNF- $\alpha$ -dependent activation of NF- $\kappa$ B in human osteoblastic HOS-TE85 cells is repressed in vector-averaged gravity using clinostat rotation. *Biochem Biophys Res Commun* 279: 258–264, 2000.
20. Leblanc A, Schneider V, Spector E, Evans H, Rowe R, Lane H, Demers L, and Lipton A. Calcium absorption, endogenous excretion, and

- endocrine changes during and after long-term bed rest. *Bone* 16, Suppl 4: 301S–304S, 1995.
21. **McAllister TN, Du T, and Frangos JA.** Fluid shear stress stimulates prostaglandin and nitric oxide release in bone marrow-derived preosteoclast-like cells. *Biochem Biophys Res Commun* 270: 643–648, 2000.
  22. **McGrath ME.** The lysosomal cysteine proteases. *Annu Rev Biophys Biomol Struct* 28: 181–204, 1999.
  23. **Miyamoto A, Shigematsu T, Fukunaga T, Kawakami K, Mukai C, and Sekiguchi C.** Medical baseline data collection on bone and muscle change with space flight. *Bone* 22, Suppl 5: 79S–82S, 1998.
  24. **Nakamura H, Kumei Y, Morita S, Shimokawa H, Ohya K, and Shinomiya K.** Suppression of osteoblastic phenotypes and modulation of pro- and anti-apoptotic features in normal human osteoblastic cells under a vector-averaged gravity condition. *J Med Dent Sci* 50: 167–176, 2003.
  25. **Ontiveros C and McCabe LR.** Simulated microgravity suppresses osteoblast phenotype, Runx2 levels and AP-1 transactivation. *J Cell Biochem* 88: 427–437, 2003.
  26. **Parhami F, Morrow AD, Balucan J, Leitinger N, Watson AD, Tintut Y, Berliner JA, and Demer LL.** Lipid oxidation products have opposite effects on calcifying vascular cell and bone cell differentiation: a possible explanation for the paradox of arterial calcification in osteoporotic patients. *Arterioscler Thromb Vasc Biol* 17: 680–687, 1997.
  27. **Ramakrishnan R, Dorris D, Lublinsky A, Nguyen A, Domanus M, Prokhorova A, Gieser L, Touma E, Lockner R, Tata M, Zhu X, Patterson M, Shippy R, Sendera TJ, and Mazumder A.** An assessment of Motorola CodeLink microarray performance for gene expression profiling applications. *Nucleic Acids Res* 30: e30, 2002.
  28. **Reich KM, Gay CV, and Frangos JA.** Fluid shear stress as a mediator of osteoblast cyclic adenosine monophosphate production. *J Cell Physiol* 143: 100–104, 1990.
  29. **Sarkar D, Nagaya T, Koga K, Nomura Y, Gruener R, and Seo H.** Culture in vector-averaged gravity under clinostat rotation results in apoptosis of osteoblastic ROS 17/2.8 cells. *J Bone Miner Res* 15: 489–498, 2000.
  30. **Sonnenfeld G, Butel JS, and Shearer WT.** Effects of the space flight environment on the immune system. *Rev Environ Health* 18: 1–17, 2003.
  31. **Sorescu GP, Sykes M, Weiss D, Platt MO, Saha A, Hwang J, Boyd N, Boo YC, Vega JD, Taylor WR, and Jo H.** Bone morphogenic protein 4 produced in endothelial cells by oscillatory shear stress stimulates an inflammatory response. *J Biol Chem* 278: 31128–31135, 2003.
  32. **Torday JS.** Parathyroid hormone-related protein is a gravisensor in lung and bone cell biology. *Adv Space Res* 32: 1569–1576, 2003.
  33. **Van Loon JJWA, Bervoets DJ, Burger EH, Dieudonne SC, Hagen JW, Semeins CM, Doulabi BZ, and Veldhuijzen JP.** Decreased mineralization and increased calcium release in isolated fetal mouse long bones under near weightlessness. *J Bone Miner Res* 10: 550–557, 1995.
  34. **Vermeer C, Wolf J, Craciun AM, and Knapen MH.** Bone markers during a 6-month space flight: effects of vitamin K supplementation. *J Gravit Physiol* 5: 65–69, 1998.
  35. **Wadhwa S, Godwin SL, Peterson DR, Epstein MA, Raisz LG, and Pilbeam CC.** Fluid flow induction of cyclo-oxygenase 2 gene expression in osteoblasts is dependent on an extracellular signal-regulated kinase signaling pathway. *J Bone Miner Res* 17: 266–274, 2002.
  36. **Wang E.** Age-dependent atrophy and microgravity travel: what do they have in common? *FASEB J* 13, Suppl: S167–S174, 1999.
  37. **Wang Y, Yang SX, Tu P, Zhang B, and Ma SQ.** Expression of parathyroid hormone (PTH)/PTH-related peptide receptor messenger ribonucleic acid in mice hair cycle. *J Dermatol Sci* 30: 136–141, 2002.
  38. **White RJ and Blomqvist CG.** Central venous pressure and cardiac function during spaceflight. *J Appl Physiol* 85: 738–746, 1998.
  39. **Whyte MP.** Hypophosphatasia and the role of alkaline phosphatase in skeletal mineralization. *Endocr Rev* 15: 439–461, 1994.
  40. **Yang X, Ji X, Shi X, and Cao X.** Smad1 domains interacting with Hoxc-8 induce osteoblast differentiation. *J Biol Chem* 275: 1065–1072, 2000.
  41. **Zaidi M, Blair HC, Moonga BS, Abe E, and Huang CL.** Osteoclastogenesis, bone resorption, and osteoclast-based therapeutics. *J Bone Miner Res* 18: 599–609, 2003.
  42. **Zayzafoon M, Gathings WE, and McDonald JM.** Modeled microgravity inhibits osteogenic differentiation of human mesenchymal stem cells and increases adipogenesis. *Endocrinology* 145: 2421–2432, 2004.
  43. **Zeeberg BR, Feng W, Wang G, Wang MD, Fojo AT, Sunshine M, Narasimhan S, Kane DW, Reinhold WC, Lababidi S, Bussey KJ, Riss J, Barrett JC, and Weinstein JN.** GoMiner: a resource for biological interpretation of genomic and proteomic data. *Genome Biol* 4(4): R28, 2003.